source: https://doi.org/10.7892/boris.141657 | downloaded: 3.4.2024

Band gap of atomically precise graphene nanoribbons as a function of ribbon length and termination

Leopold Talirz,[†,⊥] Hajo Söde,[†] Shigeki Kawai,[‡] Pascal Ruffieux,[†] Ernst Meyer,[¶,#] Xinliang Feng,[§] Klaus Müllen,[§] Roman Fasel,[†] Carlo A. Pignedoli,[*,†] and Daniele Passerone[*,†]

†*nanotech@surfaces laboratory, Empa, Swiss Federal Laboratories for Materials Science and Technology, Dübendorf, Switzerland*

‡*International Center for Materials Nanoarchitectonics, National Institute for Materials Science, 1-1, Namiki, Tsukuba, Ibaraki 305-0044, Japan.*

¶*Department of Physics, University of Basel, Switzerland.*

§*Max Planck Institute of Polymer Research, Mainz, Germany*

‖*Department of Chemistry and Biochemistry, University of Bern, Switzerland*

⊥*Laboratory of Molecular Simulation (LSMO), Institut des Sciences et Ingenierie Chimiques, Valais, École Polytechnique Fédérale de Lausanne, 1951 Sion, Switzerland*

#*Swiss Nanoscience Institute (SNI), University of Basel, Switzerland*

E-mail: carlo.pignedoli@empa.ch; daniele.passerone@empa.ch

Abstract

We study the band gap of finite $N_A = 7$ armchair graphene nanoribbons (7-AGNRs) on Au(111) through scanning tunneling microscopy/spectroscopy combined with density functional theory calculations. The band gap of 7-AGNRs with lengths of 8 nm

and more is converged to within 50 meV of its bulk value of $\approx$ 2.3eV, while the band gap opens by several hundred meV in very short 7-AGNRs. We demonstrate that even an atomic defect, such as the addition of one hydrogen atom at the termini, has a significant effect – in this case, lowering the band gap. The effect can be captured in terms of a simple analytical model by introducing an effective "electronic length".

Keywords

Graphene nanoribbons, Scanning Tunneling Spectroscopy, Density functional theory, Clar theory

Introduction

One of the driving motivations for investigating the electronic properties of two-dimensional materials, such as graphene, lies in their beneficial electrostatics for field effect transistor applications, which should enable downscaling of the channel length below conventional limits.[1] While large-scale graphene is a semimetal, quantum confinement opens an electronic band gap in graphene nanoribbons (GNRs) that depends both on the width of the ribbon and on the atomic structure of the ribbon edge.

Numerous theoretical and experimental studies have investigated the dependence of the electronic and optical properties of GNRs on their width[2–9] (see also[10] and references therein). It is typically assumed that the GNRs under investigation are long enough for their finite *length* not to play a role. Particularly in the context of experimental techniques that average over the properties of many individual nanoribbons of varying length, such as (inverse) photoemission spectroscopy, this raises the question: *How long is long enough?* More specifically, how does the electronic structure evolve from a finite molecule to the extended nanoribbon? In view of future applications in nanoscale devices, these questions are not only of academic interest.

The answer to these questions naturally depends on the physical quantities that are investigated and the accuracy that is desired. Hod and coworkers have analyzed the density of states (DOS) of finite $N_A = 9, 11$ and 13 AGNRs[11] using the HSE06 hybrid density functional.[12,13] From a comparison of the DOS for GNRs of different lengths, they conclude that the main qualitative features of the bulk electronic structure are recovered only at lengths $\gtrsim 40\,\mathrm{nm}$. This conclusion, however, depends on the assumed level broadening for the finite structures, which was chosen to be of Lorentzian form with $\Gamma = 10\,\mathrm{meV}$ width.

The bottom-up approach to GNRs, based on surface-assisted colligation and subsequent dehydrogenation of specifically designed precursor monomers, enables the synthesis of some prototypical GNRs with atomic precision.[14] Here, we investigate the evolution of their electronic structure as a function of the number of monomers that make up the ribbon. In order to focus on a simple and technologically relevant figure of merit, the discussion is restricted to the band gap Δ instead of the full DOS. Since the GNRs are synthesized with atomic precision, the experimental findings reflect intrinsic properties of the class of GNRs under study and enable direct comparison with tight binding and density functional theory calculations. In a second step, we study how adding a single hydrogen atom at the terminus affects this length dependence.

Results and Discussion

Figure 1 shows a $N_A = 7$ armchair graphene nanoribbon (7-AGNR) imaged by non-contact atomic force microscopy (AFM) as well as scanning tunneling microscopy (STM). While the long edges of the 7-AGNR are monohydrogenated, the GNRs may be terminated by one hydrogen at the central carbon atom (CH, left terminus) or by two hydrogen atoms (CH_2, right terminus), depending on the temperature T_c chosen for the dehydrogenation step.[15–17] The additional hydrogen atom can be considered an atomic defect. By varying T_c from 300° to 400°, the relative probability of CH and CH_2-termination can be tuned from a majority

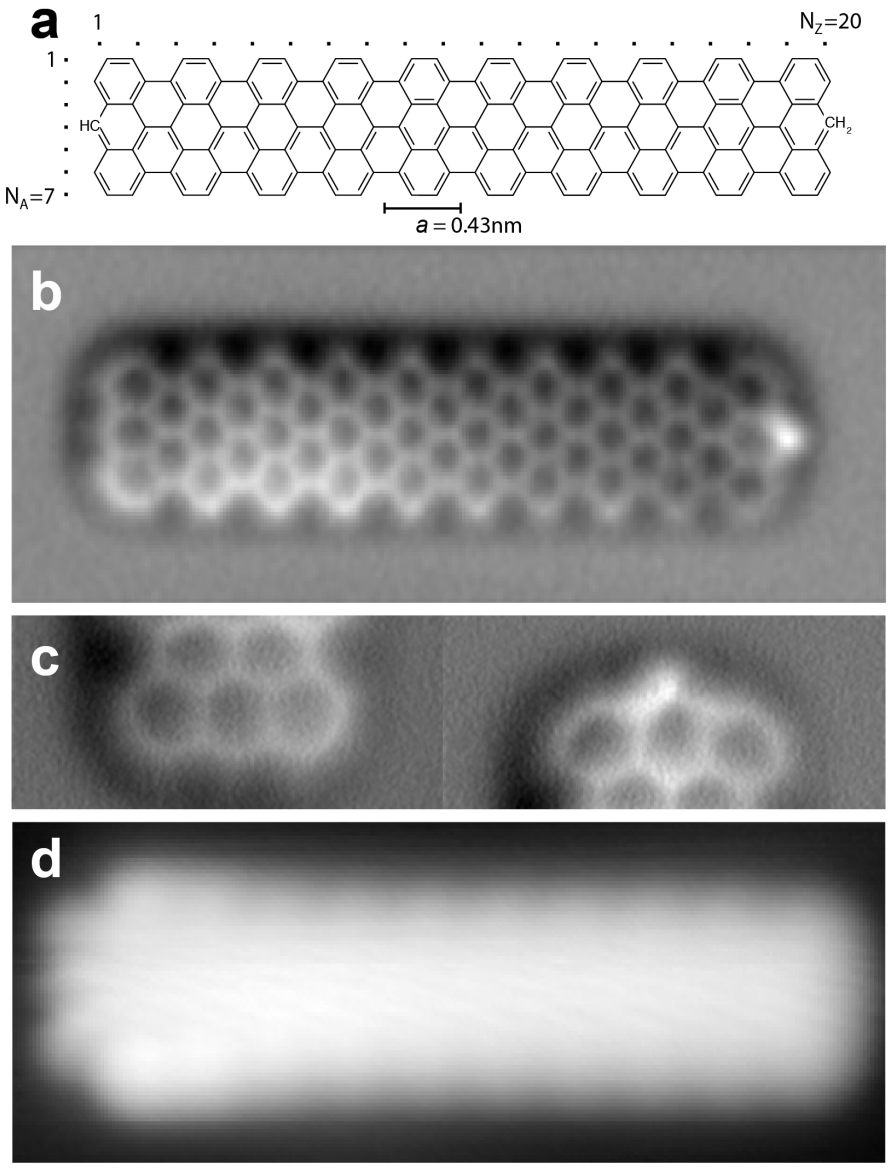

Figure 1: Atomic structure of 7-AGNR. a) Scheme of 7-AGNR with length $L = 10a \approx 4.3\,\mathrm{nm}$. b) Non-contact AFM image (oscillation amplitude A = 43 pm, bias voltage V= 0 mV). c) Zoom-in on the termini using AFM. d) Constant-current STM image (set point I=10 pA, tip bias $V_{\mathrm{tip}} = -200\,\mathrm{meV}$). All images recorded on the Au(111) surface.

of CH_2 to almost exclusively CH. Unless otherwise stated, in the following we consider only GNRs that have the same termination at both ends. Length and termination of the GNRs can be identified not only by AFM, but also by high-resolution STM,[16,17] which is the instrument used in the rest of the study. The complete knowledge of the GNRs' *atomic* structure forms the basis for the discussion of their *electronic* structure.

The band gap of finite 7-AGNRs on Au(111) was determined using scanning tunneling spectroscopy (STS). The STM tip was positioned in the center between the two termini and differential conductance spectra were recorded on a line scan across GNR using a lock-in amplifier (modulated at 860 Hz with 16 mV root-mean-square amplitude). Spectra were recorded by ramping the voltage from -1.5 V to 2.0 V at constant tip-sample distance set by $I = 0.2$ nA and $V = -1.5$ V. Following reference,[18] the band gap was extracted using the half-maximum of the valence and conduction band onsets.

This technique yields a bulk band gap of 2.3eV for 7-AGNRs on Au(111).[18] Figure 2 shows that additional confinement due to decreasing length gives rise to an increase of the band gap, as expected. For GNRs longer than 8 nm, the band gap is converged to within 50 meV. In addition to this, the data points in the length range investigated here seem to fall into one of two categories – one with higher band gap and one with lower band gap at the same length. It turns out this finding derives from differences in the termination of the ribbons under study (determined experimentally as described above): for a GNR with length $L = 10\,a \approx 4$ nm, adding a second hydrogen atom to the central carbon atom at the termini lowers the band gap by more than 0.1 eV.

In order to rationalize this observation, it is helpful to start with some basic insights into the electronic structure of graphene nanoribbons provided by Clar's theory of the aromatic sextet.[19,20] Clar's rule states that the Clar structure of a hydrocarbon that has the highest number of aromatic sextets, termed Clar *formula*, is most representative of its π-electron distribution. Figure 3 a) shows the Clar formula for the CH_2-terminated 7-AGNR. The Clar formula is unique and contains two aromatic sextets per unit cell of the GNR.[16,21] The

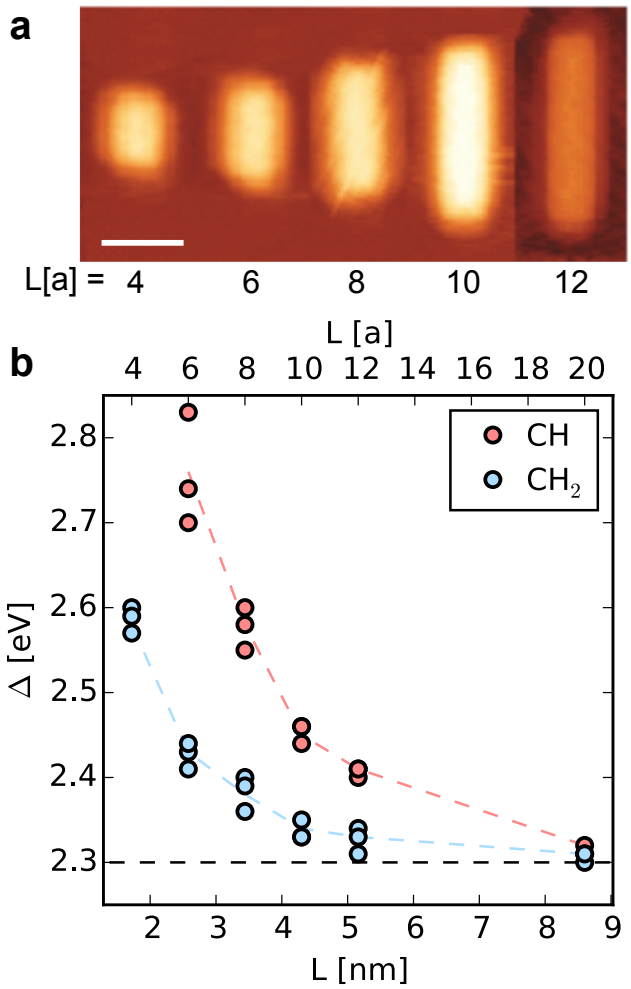

Figure 2: Band gap of 7-AGNRs. a) STM topography of finite 7-AGNRs ($V_{tip} = 1.5\,\mathrm{V}$, $I = 0.1\,\mathrm{nA}$, scale bar 2nm). b) Band gaps of 7-AGNRs as determined by scanning tunneling spectroscopy (markers). The dashed lines follow the averaged values for each length. The black dashed line at 2.3eV marks the bulk value.

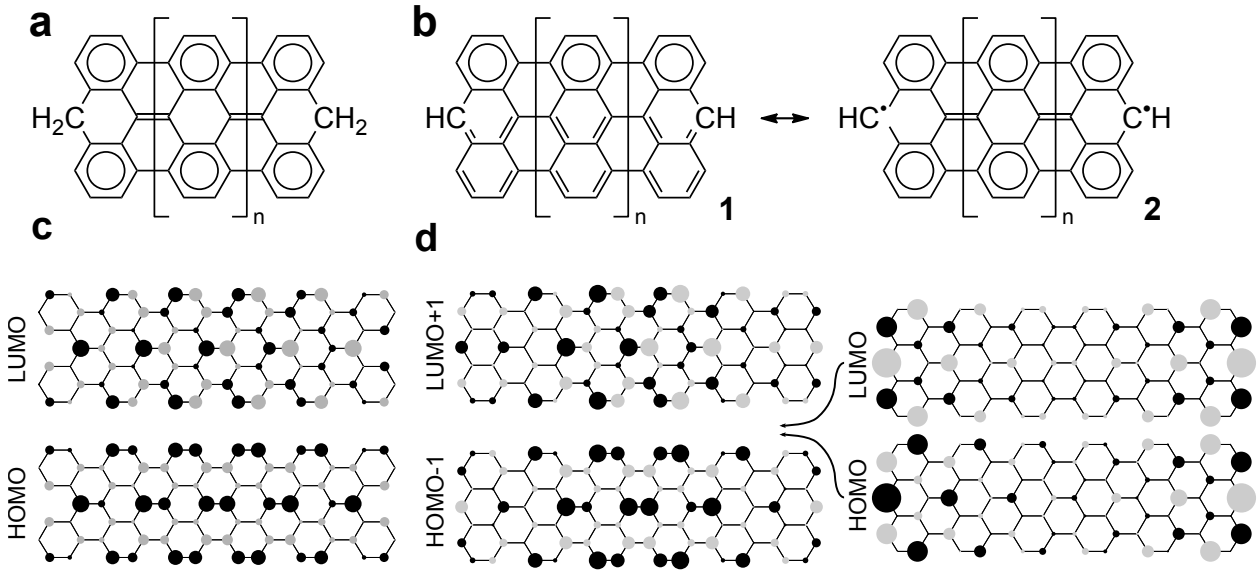

Figure 3: Electronic structure of finite 7-AGNRs. a) Clar formula for CH_2 termination. b) Clar formulas for CH termination. c) Tight binding orbitals of CH_2-terminated 7-AGNR with length $L = 6a$. The circle area is proportional to the electron density, gray/black indicates the sign of the wave function. d) Same as c), but for CH termination.

case of CH-terminated 7-AGNRs is more complicated, as shown in Figure 3 b). Multiple Clar formulae exist, but they have only one aromatic sextet per repeat unit, leading to considerably reduction in aromatic stabilization compared with the CH_2 case. At the cost of introducing one unpaired electron near each terminus of the GNR, however, a unique Clar formula with two Clar sextets per repeat unit is obtained also in this case.

The electronic structure for the CH termination is thus characterized by a competition between the cost of breaking a π-bond, favoring structure **1**, and the energetic stabilization due to increased aromaticity, favoring structure **2**. Since the aromatic stabilization increases linearly with GNR length, the question arises at which length structure **2** will dominate. Konishi et al. have studied CH-terminated 7-AGNRs of lengths $L = 2a, 3a$ and $4a$ using the complete active space self-consistent field (CASSCF) method and found a biradical character of $7, 54$ and 91% (which is in agreement with spin-unrestricted DFT calculations using the PBE functional, which find a spin-unpolarized ground state for $L = 2a$, while spin-polarization appears for $L = 3a$ and above). Further guidance on the stability of aromatic vs. radical structures is provided by thermochemistry experiments,[22] which indicate a gain

of 90 kJ/mol per aromatic ring vs. a penalty of 272 kJ/mol per couple of unpaired electrons, also corresponding to a threshold of $L = 3a$. For the length of 7-AGNRs considered here, starting from $L = 4a$, the Clar structure **2** is therefore dominant.

A simple model that captures this on a qualitative level, is tight-binding using one π-orbital per carbon atom and considering hopping only between nearest neighbors. Figure 4 (d) and (e) show frontier orbitals for a 7-AGNR of length $L = 6a$. In case of the CH_2 termination, the central carbon atom at the terminus does not contribute an electron to the π-system. Within the tight binding description, the CH_2 termination is therefore equivalent to a so-called *cove defect*, where the central carbon atom is simply removed.[23] For the CH termination instead, each terminus hosts an unpaired electron, giving rise to a highest occupied molecular orbital (HOMO) and lowest unoccupied molecular orbital (LUMO) that are exponentially localized near the terminus.[16]

Before moving from the effect of the termination on the π-electron distribution to the effect on the band gap Δ, a precise definition of Δ is required. In solid state physics, the band gap of a periodic crystal refers to the energy difference between the top of the valence band and the bottom of the conduction band. For a finite crystal, the continuous energy bands become sets of discrete energy levels and the concept of the band gap is naturally carried over to denote the energy difference between the highest such energy emerging from the valence band and the lowest such energy emerging from the conduction band.

While the corresponding electronic states remain delocalized over the crystal, the inevitable creation of surfaces can give rise to new, qualitatively different states that are exponentially localized near the surfaceand whose energies fall into the band gap between delocalized states. As discussed above, this occurs in 7-AGNRs with CH termination, which exhibit Tamm states localized at the zigzag termini. In this particular system, both the highest occupied molecular orbital (HOMO) and the lowest unoccupied molecular orbital (LUMO) are surface states of the finite one-dimensional crystal and should be disregarded when determining Δ. The bandgap of CH-terminated 7-AGNRs is therefore given by the en-

ergy difference between the LUMO+1 and the HOMO-1, while it coincides with the HOMO-LUMO gap for the CH_2 termination.

We point out that this definition of the band gap is appropriate in view of electronic transport applications, where states that are localized near the termini of the GNRs do not contribute to the current. It is also the quantity that is measured in scanning tunneling spectroscopy, when positioning the tip in the center between the two termini, as has been done in this study.

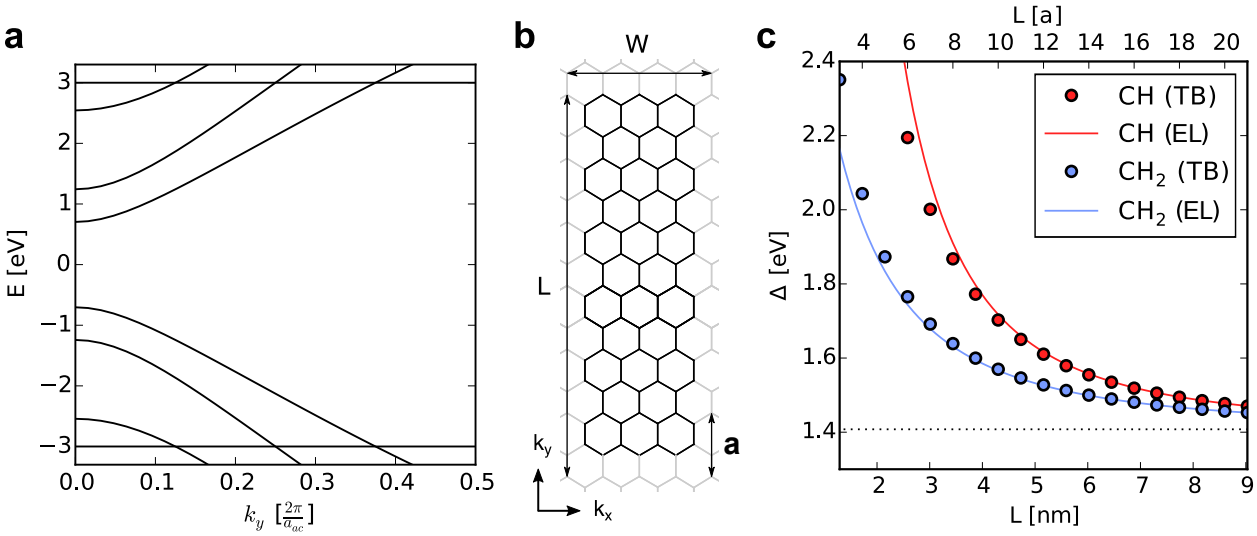

Figure 4: Electronic structure from tight binding. a) Energy bands of 7-AGNR for hopping integral $t = 3\,\text{eV}$. b) Definition of directions k_x, k_y as well as length L and width W. c) Band gap as function of length and termination (markers), as well as effective length (EL) model (line).

Figure 4 a) shows the electronic band structure of the infinite 7-AGNR. For a hopping integral of $t = 3\,\text{eV}$, a band gap of $\Delta \approx 1.41\,\text{eV}$ is obtained. This may then be compared to the band gap of 7-AGNRs with finite length L, as defined in 4 (b). Figure 4 c) demonstrates that tight binding indeed reproduces the (qualitative) experimental finding: the band gaps of CH-terminated GNRs are larger than those of CH_2-terminated GNRs of the same length.

This result might seem counterintuitive at first, since the hydrogen addition at the terminus completely removes the carbon atom from participation in the π system, i.e. the size of the π system *decreases* for CH_2-termination, which one might associate with an *in-*

crease in band gap. A closer look at the frontier orbitals shown in Figure 3 c),d) suggests a naive rationalization: considering that each carbon atom hosts one π-electron in total, the presence of highly localized states near the termini competes with the delocalized states, and may push the delocalized states in CH-terminated ribbons *inwards* compared to their counterparts in CH_2-terminated ribbons. Stronger confinement would naturally lead to a larger band gap. In the following, this observation is put on a quantitative footing using the analytic expression for the energy levels of monohydrogenated armchair and zigzag GNRs derived by Wakabayashi.[6]

The delocalized states of finite armchair graphene nanoribbons with monohydrogenated edges can be related to the dispersion of graphene $E(\vec{k})$ by finding a corresponding wave vector $\vec{k} = (k_x, k_y)$ with components k_x along the zigzag and k_y along the armchair direction. While confinement by the armchair edges gives rise to a simple discretization

$$k_x = r\frac{\pi}{W} = r\frac{2\pi}{(N_A+1)a_{zz}} \quad \text{with } r \in \{1,\ldots,N_A\} \quad , a_{zz} = 2a/\sqrt{3} \tag{1}$$

confinement in between zigzag edges results in a transcendental equation for $k_y = k_y(k_x)$.[6] In the supporting information, this equation is expanded for large length L and small k_y. For the valence and conduction bands of armchair GNRs in the semiconducting $N_A = 3p+1$ family ($p \in \mathbb{N}$), the solution for k_y takes the form

$$k_y \approx s\frac{\pi}{(N_Z+\delta)\frac{a}{2}} =: s\frac{\pi}{L+\delta'} \quad \text{with } s \in \{1,\ldots,N_Z\},\ s \ll N_Z, \tag{2}$$

$$\text{and} \quad \delta = \left[1 + 1/\left(2\cos\left[\frac{2p+1}{3p+2}\pi\right]\right)\right]^{-1} \leq 0 \tag{3}$$

In particular, we note that in the limit of large GNR lengths L, the correction term δ is independent of L and depends only on the width W of the GNR. The boundary conditions at the terminus may therefore be viewed as giving rise to an effective "electronic length" $L+\delta'$ that is *reduced* with respect to the geometric length L.

As shown in the supporting information, the band gap is then given by

$$\Delta(L) = \Delta(\infty) + \frac{C}{(L+\delta')^2} + O\left(\frac{1}{(L+\delta')^4}\right) \quad \text{for } L \to \infty. \tag{4}$$

For 7-AGNRs ($p = 2$), one obtains $\delta' = \delta\frac{a}{2} \approx -0.7\,\text{nm}$. Using a hopping integral $t = 3\,\text{eV}$, one further finds $\Delta(\infty) \approx 1.41\,\text{eV}$ and $C \approx 4.46\,\text{eVnm}^2$. The above analysis is easily generalized to GNRs of other widths. For (monohydrogenated) AGNRs of the semiconducting families $N_A = 3p$ and $N_A = 3p+1$, the discrepancy between geometric and effective electronic length grows linearly with increasing GNR width, while it takes a qualitatively different form for the quasi-metallic AGNRs with $N_A = 3p - 1$.

For the CH_2-terminated 7-AGNRs, where the analytic expressions of reference[6] do not apply, fitting equation (4) to numerical tight binding gaps of sufficiently long GNRs yields $\delta' \approx +0.9\,\text{nm}$.

Coming back to the original question, the termination can thus be viewed as influencing the effective "electronic length" of the GNR: CH_2-terminated 7-AGNRs appear $0.9 + 0.7 = 1.6\,\text{nm}$ longer than CH-terminated ones, while consisting of the same number of monomers[1] Figure 4 c) compares the exact tight binding gaps (markers) to those obtained using the "electronic length" approximation (lines). Despite being derived for the limit $L \to \infty$, the model agrees well with the full tight binding calculation in the length range relevant to this study.

While single-orbital nearest-neighbor tight binding lends itself to qualitative investigations, neglecting the variation of on-site energies,[2] hopping between more than nearest neighbors and the Coulomb repulsion between electrons[24] constitutes a serious simplification. In this respect, an *ab initio* scheme, such as density functional theory, presents a significant step forward. For the case of 7-AGNRs, it has been found that the effective single-particle description of spin-unrestricted Kohn-Sham DFT with a semi-local functional is able to cap-

[1] This refers to valence and conduction band. See the supporting information for computing δ' for other bands.

ture the essential features when compared to a solution of the many-body Hubbard model.[24] We have computed the band gaps of finite 7-AGNRs consisting of $4, 6, \ldots, 20$ anthene units using the PBE functional,[25] both for CH and CH_2 termination (see methods section for details).

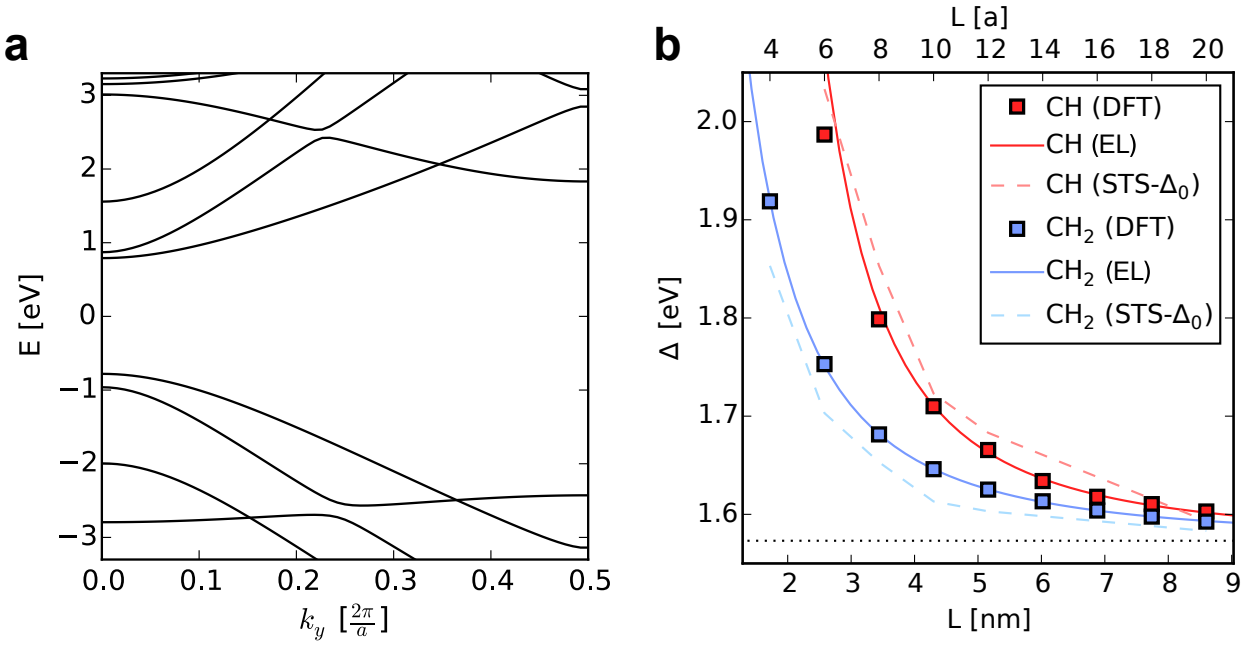

Figure 5: DFT electronic structure. a) Energy bands of 7-AGNR. The center of the gap has been shifted to zero energy. b) DFT band gap as function of length and termination. Dashed lines are averaged experimental values from Figure 2, decreased by a constant $\Delta_0 = 0.73\,\text{eV}$ to aid comparison. The dotted line marks the bulk value of the DFT gap at 1.57 eV.

The resulting Kohn-Sham gaps are shown in Figure 5 (b). The continuous lines are obtained by fitting $\Delta(L)$ against equation (4), while fixing $\Delta(\infty) = 1.57\,\text{eV}$ to the value of the bulk band gap.[2] Similar to tight binding, one finds $\delta' \approx -0.7\,\text{nm}$ for the CH termination and $\delta' \approx +0.5\,\text{nm}$ for the CH_2 termination, while the values for C are significantly reduced due to the weaker dispersion of the DFT bands in 5 a) compared to tight binding.

Figure 5 (b) also shows the experimental band gaps obtained from STS (dashed lines).

[2]The least-squares fit was performed in the range of $L \in [12a, 20a]$. The values with standard errors are $\delta' = -0.67 \pm 0.14\,\text{nm}$, $C = 1.81 \pm 0.12\,\text{nm}$ (CH) and $\delta' = +0.47 \pm 0.08\,\text{nm}$, $C = 1.66 \pm 0.05\,\text{nm}$ (CH_2).

To aid the comparison, the experimental data have been reduced by a constant shift of

$$\Delta_0 = \Delta 2.3\,\mathrm{eV} - 1.57\,\mathrm{eV} = 0.73\,\mathrm{eV} \quad , \tag{5}$$

letting both gaps agree in the limit of $L \to \infty$.

Kohn-Sham DFT with approximate semi-local exchange-correlation functionals is well-known to underestimate band gaps of molecules and bulk semiconductors. The size of this error will, in general, depend on the atomic structure of the system under investigation. Yet, Figure 5 (b) suggests that a constant shift by Δ_0 brings the PBE Kohn-Sham gap of finite 7-AGNRs with different lengths and terminations into good agreement with experiment.

While there may be no general justification for applying such a constant shift, we note that for the 7-AGNR the *dispersion* of the frontier electronic bands in DFT fits the experimentally determined dispersion rather well.[26] If the opening of the band gap in finite 7-AGNRs arises mainly through the corresponding discretization of the bulk frontier bands,[3] it then follows that the difference Δ_0 between experimental and Kohn-Sham gap is independent of length.

Finally, while the electronic band gap of the 7-AGNR converges already for short segments, we note that this differs from GNRs in the so-called quasi-metallic family of width $W = (N_A+1)a_{zz}$ with $N_A = 3p+2$. As discussed in reference,[27] segments beyond 30 nm are necessary to converge the electronic band gap for ribbons in this family due to the smaller effective mass of the charge carriers involved.

Conclusions

The band gap of finite 7-AGNRs has been analyzed as a function of length and termination through scanning tunneling spectroscopy of atomically precise 7-AGNRs on Au(111). The combination with tight binding and density functional theory calculations provides a ratio-

[3] On the experimental side, this may depend significantly on the screening from the underlying Au surface. For GNRs on insulators and, even more so, for free-standing GNRs, an appropriate treatment of many-body effects should become necessary – for example, within the *GW* approximation.

nalization of the significant difference observed between GNR terminations. The difference can be expressed in terms of an effective "electronic length" $L + \delta'$ of the ribbon, which differs from the geometric length L by a shift δ' that depends on the boundary conditions at the CH_2 or CH terminus.

In agreement between tight binding, DFT and experiment, CH-terminated ribbons effectively appear more than 1 nm *shorter* compared their CH_2-terminated counterparts with the same number of monomers, giving rise to a larger band gap of short CH-terminated 7-AGNRs according to the formula $\Delta(L) = \Delta(\infty) + \frac{C}{(L+\delta')^2}$ and illustrating the sensitivity of the π-electronic structure of GNRs even to single atomic defects.

While simple simple computational schemes can provide valuable insight into trends in the electronic properties of this class of nanomaterials as a function of their size and termination, quantitative predictions for device applications call for higher-level methods that include the dielectric screening by the substrate.

Acknowledgement

Calculations were supported by a grant from the Swiss National Supercomputing Centre (CSCS) under project ID s746. The Swiss National Science Foundation and the Swiss National Centre for Computational Design and Discovery of Novel Materials (MARVEL) are acknowledged for financial support. The work of S. K. is supported in part by Japan Society for the Promotion of Science (JSPS) KAKENHI Grant Number 19H00856.

The authors thank both reviewers for their thorough reading of the manuscript and for their constructive feedback.

Methods

All measurements were performed with a commercially available Omicron low temperature scanning tunneling microscopy (STM)/atomic force microscopy (AFM) system, operating

in ultra-high vacuum at 4.8 K. We used a tuning fork with a chemically etched tungsten tip as a force sensor.[28] The resonance frequency and the mechanical quality factor were 23067.3 Hz and 26704 Hz, respectively. The high stiffness of 1800 N/m allows for stable operation with small amplitude.[29] The frequency shift, caused by the tip-sample interaction, was detected with a commercially available digital phase-locked loop (Nanonis: OC-4 and Zurich Instruments: HF2-LI and HF2-PLL).[30] For the STM measurement, the bias voltage was applied to the tip while the sample was electronically grounded. The tip apex was sharpened ex situ by milling with a focused ion beam. The tip radius was less than 10 nm. A clean gold tip was formed in situ by indenting to the Au sample surface and applying several bias voltage pulses between tip and sample. For AFM, the tip apex was terminated with a CO molecule, which was picked up from the surface.[31] Clean Au(111) surfaces were prepared in situ by repeated cycles of standard Ar^+ sputtering (3×10^{-6} mbar, 1000 eV, and 15 min) and annealing at 720 K. 7-AGNRs were grown under ultrahigh vacuum conditions (base pressure $1 \times 10^{-10} mbar$) using 10,10‘-dibromo-9,9‘-bianthryl (DBBA) as precursor monomer, as reported previously.[14] After deposition of DBBA on the Au(111) surface held at room temperature, polymerization and subsequent cyclodehydrogenation were induced by annealing to 300 C (400 C) to obtain 7-AGNRs with a majority of CH_2 (CH) termination. Identification of termination was accomplished by scanning at low bias, where CH-terminated 7-AGNRs exhibit a specific density of states pattern at the ribbon termini.[16]

Spin-unrestricted DFT calculations have been performed with the PBE generalized gradient approximation to the exchange-correlation functional.[25] The Quantum ESPRESSO package[32] was used, together with projector augmented-wave ultrasoft pseudopotentials from the `pslibrary.1.0.0`[33] and an energy cutoff of 46 Ry for the wave functions and 326 Ry for the charge density. Atomic positions were relaxed until the forces were below 10^{-4} Hartree atomic units. The band structure of the periodic 7-AGNR was calculated using 64 k-points in the first Brillouin zone.

TOC entry

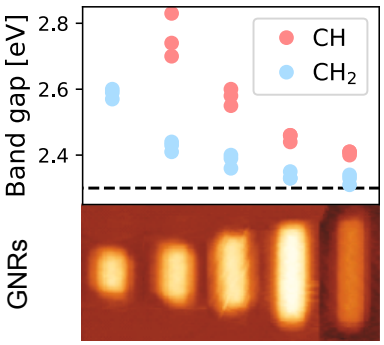

The band gap of atomically precise GNRs with lengths in the sub-10nm regime varies significantly both with their length and termination.

References

(1) Schwierz, F. Graphene transistors. *Nat. Nanotechnol.* **2010**, *5*, 487–96.

(2) Son, Y.-W.; Cohen, M. L.; Louie, S. G. Energy Gaps in Graphene Nanoribbons. *Phys. Rev. Lett.* **2006**, *97*, 216803.

(3) Prezzi, D.; Varsano, D.; Ruini, A.; Marini, A.; Molinari, E. Optical properties of graphene nanoribbons: The role of many-body effects. *Phys. Rev. B* **2008**, *77*, 041404.

(4) Yang, X.; Dou, X.; Rouhanipour, A.; Zhi, L.; Räder, H. J.; Müllen, K. Two-Dimensional Graphene Nanoribbons. *J. Am. Chem. Soc.* **2008**, *130*, 4216–4217.

(5) Yazyev, O. V. Emergence of magnetism in graphene materials and nanostructures. *Rep. Prog. Phys.* **2010**, *73*, 056501.

(6) Wakabayashi, K.; Sasaki, K.-i.; Nakanishi, T.; Enoki, T. Electronic states of graphene nanoribbons and analytical solutions. *Sci. Technol. Adv. Mater.* **2010**, *11*, 054504.

(7) Zhu, X.; Su, H. Scaling of Excitons in Graphene Nanoribbons with Armchair Shaped Edges. *J. Phys. Chem. A* **2011**, *115*, 11998–12003.

(8) Kimouche, A.; Ervasti, M. M.; Drost, R.; Halonen, S.; Harju, A.; Joensuu, P. M.; Sainio, J.; Liljeroth, P. Ultra-narrow metallic armchair graphene nanoribbons. *Nat. Commun.* **2015**, *6*, 10177.

(9) Kharche, N.; Meunier, V. Width and Crystal Orientation Dependent Band Gap Renormalization in Substrate-Supported Graphene Nanoribbons. *J. Phys. Chem. Lett.* **2016**, *7*, 1526–1533.

(10) Talirz, L.; Pignedoli, C. A. In *Handbook of Materials Modeling*; Andreoni, W., Yip, S., Eds.; Springer International Publishing: Cham, 2018; pp 1–35.

(11) Hod, O.; Peralta, J.; Scuseria, G. Edge effects in finite elongated graphene nanoribbons. *Phys. Rev. B* **2007**, *76*, 4–7.

(12) Heyd, J.; Scuseria, G. E.; Ernzerhof, M. Hybrid Functionals Based on a Screened Coulomb Potential. *J. Chem. Phys.* **2003**, *118*, 8207–8215.

(13) Heyd, J.; Scuseria, G. E.; Ernzerhof, M. Erratum: "Hybrid Functionals Based on a Screened Coulomb Potential" [J. Chem. Phys.118, 8207 (2003)]. *J. Chem. Phys.* **2006**, *124*, 219906.

(14) Cai, J.; Ruffieux, P.; Jaafar, R.; Bieri, M.; Braun, T.; Blankenburg, S.; Muoth, M.; Seitsonen, A. P.; Saleh, M.; Feng, X.; Müllen, K.; Fasel, R. Atomically precise bottom-up fabrication of graphene nanoribbons. *Nature* **2010**, *466*, 470–3.

(15) Blankenburg, S.; Cai, J.; Ruffieux, P.; Jaafar, R.; Passerone, D.; Feng, X.; Müllen, K.; Fasel, R.; Pignedoli, C. A. Intraribbon Heterojunction Formation in Ultranarrow Graphene Nanoribbons. *ACS Nano* **2012**, *6*, 2020–2025.

(16) Talirz, L.; Söde, H.; Cai, J.; Ruffieux, P.; Blankenburg, S.; Jafaar, R.; Berger, R.; Feng, X.; Müllen, K.; Passerone, D.; Fasel, R.; Pignedoli, C. A. Termini of bottom-up fabricated graphene nanoribbons. *J. Am. Chem. Soc.* **2013**, *135*, 2060–2063.

(17) van der Lit, J.; Boneschanscher, M. P.; Vanmaekelbergh, D.; Ijäs, M.; Uppstu, A.; Ervasti, M.; Harju, A.; Liljeroth, P.; Swart, I. Suppression of electron-vibron coupling in graphene nanoribbons contacted via a single atom. *Nat. Commun.* **2013**, *4*, 2023.

(18) Ruffieux, P.; Cai, J.; Plumb, N.; Patthey, L.; Prezzi, D.; Ferretti, A.; Molinari, E.; Feng, X.; Müllen, K.; Pignedoli, C. A.; Fasel, R. Electronic Structure of Atomically Precise Graphene Nanoribbons. *ACS Nano* **2012**, *6*, 6930–6935.

(19) Clar, E. *The aromatic sextet*; J. Wiley: London, New York, 1972.

(20) Wassmann, T.; Seitsonen, A. P.; Saitta, A. M.; Lazzeri, M.; Mauri, F. Clar's Theory, π-Electron Distribution, and Geometry of Graphene Nanoribbons. *J. Am. Chem. Soc.* **2010**, *132*, 3440–3451.

(21) Konishi, A.; Hirao, Y.; Kurata, H.; Kubo, T. Investigating the edge state of graphene nanoribbons by a chemical approach: Synthesis and magnetic properties of zigzag-edged nanographene molecules. *Solid State Commun.* **2013**, *175-176*, 62–70.

(22) Yeh, C.-N.; Chai, J.-D. Role of Kekulé and Non-Kekulé Structures in the Radical Character of Alternant Polycyclic Aromatic Hydrocarbons: A TAO-DFT Study. *Sci. Rep.* **2016**, *6*, 30562.

(23) Wakabayashi, K.; Okada, S.; Tomita, R.; Fujimoto, S.; Natsume, Y. Edge States and Flat Bands of Graphene Nanoribbons with Edge Modification. *J. Phys. Soc. Jpn.* **2010**, *79*, 034706.

(24) Ijäs, M.; Ervasti, M.; Uppstu, A.; Liljeroth, P. Electronic states in finite graphene nanoribbons: Effect of charging and defects. *Phys. Rev. B* **2013**, 1–14.

(25) Perdew, J. P.; Burke, K.; Ernzerhof, M. Generalized Gradient Approximation Made Simple. *Phys. Rev. Lett.* **1996**, *77*, 3865–3868.

(26) Söde, H.; Talirz, L.; Gröning, O.; Pignedoli, C. A.; Berger, R.; Feng, X.; Müllen, K.; Fasel, R.; Ruffieux, P. Electronic band dispersion of graphene nanoribbons via Fourier-transformed scanning tunneling spectroscopy. *Phys. Rev. B* **2015**, *91*, 045429.

(27) Wang, S.; Kharche, N.; Costa Girão, E.; Feng, X.; Müllen, K.; Meunier, V.; Fasel, R.; Ruffieux, P. Quantum Dots in Graphene Nanoribbons. *Nano Lett.* **2017**, *17*, 4277–4283.

(28) Giessibl, F. J. High-speed force sensor for force microscopy and profilometry utilizing a quartz tuning fork. *Appl. Phys. Lett.* **1998**, *73*, 3956–3958.

(29) Giessibl, F. J. Advances in atomic force microscopy. *Rev. Mod. Phys.* **2003**, *75*, 949–983.

(30) Albrecht, T. R.; Grütter, P.; Horne, D.; Rugar, D. Frequency modulation detection using high-Q cantilevers for enhanced force microscope sensitivity. *J. Appl. Phys.* **1991**, *69*, 668–673.

(31) Bartels, L.; Meyer, G.; Rieder, K.-H. Controlled vertical manipulation of single CO molecules with the scanning tunneling microscope: A route to chemical contrast. *Appl. Phys. Lett.* **1997**, *71*, 213–215.

(32) Giannozzi, P. et al. QUANTUM ESPRESSO: a modular and open-source software project for quantum simulations of materials. *J. Phys. Condens. Matter* **2009**, *21*, 395502.

(33) Dal Corso, A. Pseudopotentials Periodic Table: From H to Pu. *Comput. Mater. Sci.* **2014**, *95*, 337–350.